Journal of Power Sources 226 (2013) 8–15

Contents lists available at SciVerse ScienceDirect

Journal of Power Sources

journal homepage: www.elsevier.com/locate/jpowsour

A novel TiO_2 nanowires/nanoparticles composite photoanode with SrO shell coating for high performance dye-sensitized solar cell

Qin Hu, Congcong Wu, Liqiang Cao, Bo Chi*, Jian Pu, Li Jian

School of Materials Science and Engineering, State Key Lab of Material Processing and Die & Mould Technology, Huazhong University of Science and Technology, Wuhan 430074, China

HIGHLIGHTS

- TiO_2 nanowire/nanoparticle composite photoanode with SrO shell is prepared.
- The composite photoanode PW10 obtains high conversion efficiency (η) of 6.27%.
- SrO shell on composite photoanode can further improve η to 6.91%.

ARTICLE INFO

Article history:
Received 27 July 2012
Received in revised form
17 October 2012
Accepted 19 October 2012
Available online 29 October 2012

Keywords:
Dye-sensitized solar cells
Nanowire
Shell coating
Electron recombination

ABSTRACT

Dye-sensitized solar cell (DSSC) based on TiO_2 nanowires/nanoparticles composite photoanode with SrO shell coating is studied. TiO_2 nanowires are synthesized by hydrothermal treatment and the composite photoanodes are prepared through mixing various mass ratios of nanowires and nanoparticles. The result shows that the composite photoanode containing optimized TiO_2 nanoparticles and nanowires can increase electron transfer efficiency. DSSC with PW10 (nanowires content is 10 wt%) photoanode shows a relative high conversion efficiency of 6.27% because of the synergistic role of the high specific area of nanoparticles and rapid electron transfer of nanowires. Furthermore, PW10 photoanode with SrO shell coating can increase the conversion efficiency to 6.91% due to the barrier role of the shell. The research confirms that such a novel photoanode structure can suppress the electrons recombination process and increase the conversion efficiency effectively.

1. Introduction

Since the power conversion efficiency (PCE) of 7.1% under AM 1.5 illumination was reported by Grätzel and co-workers in 1991, dye-sensitized solar cells (DSSCs) have attracted much attention owing to their high efficiency with low cost and environment friendly preparation [1,2]. A porous nanocrystalline TiO_2 film is usually employed as the photoanode of DSSC for absorbing dye molecules, which plays an important role in the light harvesting efficiency of DSSC [3]. A high performance DSSC requires nanoscale and highly crystalline TiO_2 electrodes with large surface areas and favorable electrical contiguity with conducting glass substrates, so that dyes can be sufficiently adsorbed and electrons can be quickly transferred [4]. It is confirmed that photoanode film with one-dimensional nano-structure has been proven to be an effective way to facilitate electron transportation [5–10]. Law et al. found the electron diffusion coefficient of ZnO nanowires is several hundred times larger than that of ZnO or TiO_2 nanoparticles film [10]. However, photoanode with one-dimensional nano-structure as ZnO nanorods or TiO_2 nanotubes shows a very low surface area compared with the porous nanoparticles TiO_2 photoanode, which will result in low dye molecule adsorption and further decrease the photo-to-electric efficiency. Kurata et al. [11] showed that 8.52% PCE could be achieved by a complex DSSC electrode made of titania nanorods mixed with P25 nanoparticles. Therefore, photoanode with one-dimensional nano-structure mixed with P25 nanoparticles is proven to be an effective way to improve overall cell performance.

Moreover, DSSC still suffers from a high recombination rate between the injected electrons and the acceptor species in electrolyte. One amazing idea is using photoanode with core/shell structure that can suppress the recombination and reduce the electrons loss. In such structure, a wide-band gap semiconductor coating is covered on the surface of the porous TiO_2 film, to form a composite core–shell structure of the photoanode, with no change of the nature of the anode. Since the introduction of such

* Corresponding author. Tel./fax: +86 27 8755 8142.
E-mail address: chibo@hust.edu.cn (B. Chi).

0378-7753/$ – see front matter © 2012 Elsevier B.V. All rights reserved.
http://dx.doi.org/10.1016/j.jpowsour.2012.10.066

structure can effectively suppress the recombination rate between electrons and the triiodide in the electrolyte, the loss of electrons transfer is reduced [12–15]. This photoanode with core/shell structure involves energy gradient approach [13], in which the two materials differ by their conduction band potential [16–18]. Arranging these materials in the correct geometry is expected to drive the electrons to the desired direction by energy considerations.

Herein we propose a novel hybrid photoanode composition of the one-dimensional nanowires and conventional nanoparticles TiO_2, with a wide-band gap semiconductor SrO ($E_g = 5.7$ eV) as the shell coating. The schematic of the configuration of DSSC structure is shown in Fig. 1. In such a photoanode structure, TiO_2 nanowires can promote the rapid electrons transfer and enhance the light scattering effect, and nanoparticles can increase the specific surface area for the absorption of more dyes, while SrO shell coating can suppress the recombination of the photo-generated electrons with triiodide in the electrolyte. Thus the electrons transfer and the photo-to-electric conversion efficiency will be enhanced effectively by this novel photoanode.

In present study, the one-dimensional TiO_2 nanowires (NWs) are prepared by hydrothermal treatment and TiO_2 nanoparticles (NPs) are commercially available. The effect of the mass ratio of NWs and NPs on the performance of DSSCs is investigated. Moreover, the coating of SrO shell on the hybrid nano-structure is also fabricated for further suppressing the electrons recombination. The effect of the shell coating thickness on the cell performance is optimized and the enhancement mechanism is also discussed.

2. Experimental section

2.1. Synthesis of TiO_2 nanowires

A total of 0.2 g of commercial TiO_2 powders (Degussa P25) was mixed with 80 mL 8 M KOH aqueous solution in the Teflon-lined autoclave and heated at 180 °C for 22 h. Then the samples were washed with 0.1 M HCl solution and distilled water, until the pH of the solution was adjusted to 7. After dried at 60 °C, the samples were calcined in the air at 450 °C for 2 h.

2.2. Preparation of TiO_2 nano-composites

The as-prepared TiO_2 NWs were mixed with commercial TiO_2 P25 NPs. Four pastes containing different mixing ratio of NPs and NWs were prepared with 0, 10, 20, and 100 wt% NWs in the mixture, respectively (labeled as PW0, PW10, PW20, and PW100). The mixed TiO_2 NWs and NPs were dispersed in α-terpineol as solvent and ethyl cellulose as binder. And TiO_2 nano-composite were then prepared using the screen printing technique followed by calcination of the composite TiO_2 films at 450 °C for 1.5 h.

2.3. SrO shell coating preparation

SrO shell coating was prepared on TiO_2 NWs and NPs composite using the dip-coating method. In typical process, the shell coatings were coated by dipping the composite into saturated $Sr(NO_3)_2$ aqueous solution, and then washed thoroughly with distilled water. After dried, the samples were calcined in the air at 450 °C for 0.5 h. The thickness of SrO shell coating was controlled by the dipping time.

2.4. Cell assembly

TiO_2 nano-composite films with and without SrO shell were also immersed into 0.5 mM N719 dye in anhydrous ethanol at room temperature for 24 h. The counter electrode was a Pt-coated FTO glass produced by coating H_2PtCl_6 solution onto FTO glass followed by heating at 450 °C for 1 h. The active area of DSSC is 0.1963 cm^2 and the electrolyte is the mixture of 0.2 M DMPII, 0.5 M LiI, 50 mM I_2, and 0.5 M 4-TBP in 3-MPN.

2.5. Measurement and characterization

The crystallinities of TiO_2 nano-composites with and without SrO shell coating were investigated using X-ray diffraction (XRD, X'Pert pro. PANalytical B.V). The morphologies were investigated using a field emission scanning electron microscope (FE-SEM, FEI, Sirion 200). The formation of SrO shell on TiO_2 nano-composites was examined using a transmission electron microscope (TEM, FEI, Tecnai G220), X-ray energy dispersive spectrometer (EDAX) and X-ray photoelectron spectroscopy (XPS, ThermoVG, Sigma Probe). Photocurrent–voltage measurements and electrochemical impedance spectroscopy (EIS) were performed using a 1287 Electrochemical Interface coupled with 1260 Frequency Response Analyzers (Solartron Analytical.) under AM 1.5G of simulated sunlight (Newport 91160, 300 W with air mass 1.5 global filter).

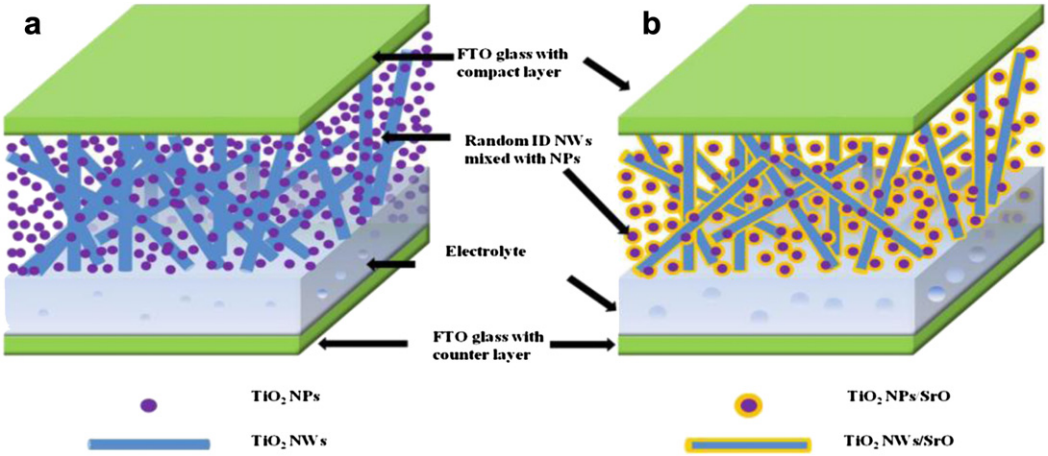

Fig. 1. Schematic configuration of DSSC based on composite of NWs/NPs without (a) and with SrO shell coating (b).

3. Results and discussion

3.1. XRD

Fig. 2 shows the XRD patterns of P25 (a), nanowire sample synthesized by hydrothermal treatment at 180 °C for 22 h (b) and as-prepared sample with a SrO shell (c). P25 shows typical diffraction peaks of anatase and rutile. However it can be found that the as-prepared sample with and without SrO shell are almost pure anatase structure. And small diffraction peaks assigned to $K_2Ti_2O_5$ are also observed, which may be due to the inadequate removement of K^+ during the ions exchange process. In the hydrothermal treatment process, P25 powder reacts with high concentration OH^- ions and forms $K_2Ti_2O_5$ [19]. During the acid-treatment, most of K^+ ions are exchanged by H^+ to form $H_2Ti_2O_5 \cdot H_2O$. Then after calcined at 450 °C for 2 h, $H_2Ti_2O_5 \cdot H_2O$ is converted to pure anatase TiO_2.

3.2. SEM

Fig. 3 shows SEM images of the synthesized NWs by hydrothermal process at 180 °C for 22 h in 8 M KOH after washing with 0.1 M HCl solution. The uncalcined $H_2Ti_2O_5 \cdot H_2O$ (Fig. 3a) shows typical nanowire structure with NWs aggregating together. And the morphology of P25 nanoparticles cannot be observed again. Nanowires can be found with diameter ranging from tens to hundreds nanometers. After calcined at 450 °C for 2 h, as shown in Fig. 3b, the as-prepared TiO_2 NWs can be obtained without apparently changing the morphological appearance. However, it is obvious that the diameter of NWs increases a little after calcination. Most of these NWs have the length of a few microns.

3.3. TEM

Fig. 4 presents the TEM results of the samples after washed with 0.1 M HCl solution and calcined at 450 °C for 2 h. It can be found that the nanowire has smooth surface after calcination, with nearly uniform in diameter along its length, which suggests that the nanowire grows through epitaxial addition of growth units to the tips [20]. The SAED patterns (inset) indicate that TiO_2 nanowire is of single crystalline morphology. The formation mechanism of NWs has been discussed in our previous work [21]. However, it is difficult to find the shell coating on the nanowires or nanoparticles for the coated samples in TEM images, which may due to the thin coating thickness.

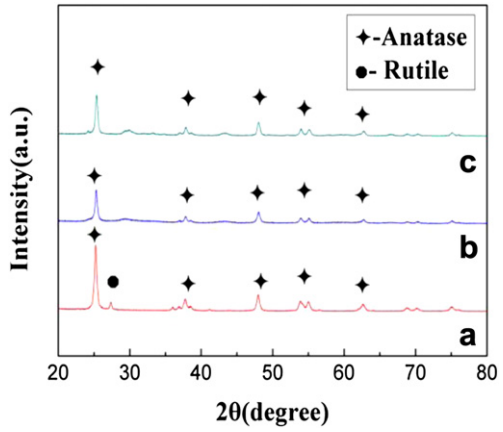

Fig. 2. XRD patterns of P25 (a) and sample synthesized by hydrothermal treatment at 180 °C for 22 h (b), and as-prepared sample with a SrO shell (c).

3.4. EDX

Fig. 5 shows EDX result of TiO_2 nano-composite with SrO shell coating. In the TEM results, it has been confirmed that SrO shell coating is hard to be observed due to its thin thickness and serious reunion. However, the EDX result shows that the measured sample contains element Sr, which comes from the shell coating. The result confirms the existing of Sr in the sample. Other elements are also observed, as K is the residue from the incomplete exchange process, and Cu, C, Si may come from the support.

3.5. XPS

The surface composition of the as-prepared sample with SrO shell is also investigated by XPS, as shown in Fig. 6. The binding energies (BEs) in the XPS spectra are calibrated by using BE of C 1*s* (284.6 eV). It can be found that all of the peaks on the curve are ascribed to Sr, Ti, O, and C elements. And no peaks of other elements are observed. The presence of C mainly comes from pump oil due to vacuum treatment before measurement. Therefore, it is concluded that the SrO shell coating sample only contains Sr, Ti, and O, which is in good agreement with the above EDX result. In Fig. 6a, O 1*s* profile is asymmetric and can be fitted to two symmetrical peaks (locating at 529.45 eV and 531.0 eV), indicating two different kinds of O species in the sample. According to their BEs, the main line is assigned to O^{2-} ion of the metal oxide [22]. The peak at 529.45 eV arises from the lattice oxygen (O—Ti—O) [23] and the peak at 531.0 eV is mainly from Sr oxide, which will be further confirmed by the Sr 3*d* emission. The Sr 3*d* XPS spectra, as shown in Fig. 6b, has main peak with BE of 133.9 eV, which can be assigned as Sr 3*d*5/2 line. The result is in good agreement with BE data for Sr in the literature [24–26]. Fig. 6c shows a main doublet for Ti (IV) composing of two symmetric peaks situated at BE of 458.30 eV (Ti 2*p*3/2) and BE of 464.00 eV (Ti 2*p*1/2), which is in agreement with the literature [27,28].

3.6. Characterization of photoanodes

Morphologies of films made from PW0, PW10, and PW20 pastes are shown in Fig. 7. It can be found that films of PW0, PW10, and PW20 are porous with void spaces from the aggregation of the individual nanoparticles. In NWs mixed samples of PW10 and PW20, NWs are well dispersed into the nanoparticles. The NW/NP composites are connected tightly to form a porous network structure. However, with the increase of the content of NWs, the film becomes loose and shows less compact structure with large void spaces of several hundred nanometers in size, which may cause a significant decrease of specific surface area. From the result we can learn that the mass rate of NWs in the composite photoanode has an import role in the specific surface area and the porosity of the composites, which could affect the performance of DSSC [29].

3.7. Cell performance

3.7.1. Cell with NWs/NPs

The effect of NWs/NPs composite on the performance of nanoporous electrode is measured and analyzed. The performances of DSSCs based on these composite nanoporous photoanode are measured under simulated sunlight and under dark condition respectively. Fig. 8a shows the photocurrent-voltage dependences (*I*–*V* curves) of DSSCs with PW0, PW10, PW20, and PW100 photoanode. The corresponding photo–electric parameters are summarized in Table 1. As can be seen from the table, when the content of NWs is 0 wt% (with only NPs), the cell shows open circuit voltage (V_{oc}) of 0.773 V, short circuit current (J_{sc}) of 14.68 mA cm^{-2},

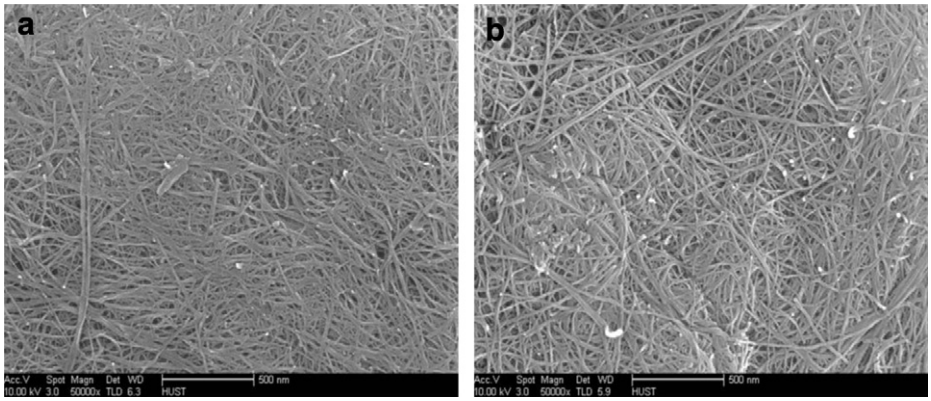

Fig. 3. SEM image of NWs before (a) and after calcination at 450 °C for 2 h (b).

and conversion efficiency (η) of 5.62%. When NWs content reaches to 10 wt%, the corresponding V_{oc}, J_{sc}, and η increases to 0.780 V, 16.02 mA cm^{-2}, and 6.27%. Further increasing the content of NWs to 20 wt%, the corresponding V_{oc} increases to 0.791 V, but the performance of the cell is not improved accordingly. DSSC with the pure NWs photoanode (PW100) shows worse performance than those NWs/NPs photoanodes, which can be due to the low surface area of the pure NWs photoanode. The results show that appropriate content of NWs can improve the cell performance and the addition of NWs should be confined into a reasonable content.

Compared with NPs, NWs have higher charge transportation rate, though the specific surface area of NWs is lower than that of NPs. Moreover, photo-generated carriers travelling along the one-dimensional long axis can reduce the possible loss of photoelectron and increase the performance of the cell. However, as discussed previous, the addition of NWs into NPs may decrease the specific surface area. Thus, appropriate content of NWs added into nanoparticles may completely increase the performance, especial the conversion efficiency.

To further confirm the role of NWs addition, cells under dark condition are measured to investigate the charge back reaction characteristics. Fig. 8b shows the performance curves of DSSCs consisting of PW0, PW10, PW20, and PW100 photoanode under dark condition. At the same applied bias voltage, dark currents of NWs/NPs composite photoanodes are smaller than pure TiO_2 NPs photoanode. Among the photoanodes with NWs addition, PW100 shows the smallest dark current, indicating that the charge back recombination rate is the lowest in PW100 photoanode, which is owing to fewer defects, faster average electron transport rate, and lower electron recombination of NWs. Thus, we can infer that the incorporation of NWs into NPs can promote the electrons transportation and suppress the recombination effectively, and furthermore, increase the cell performance, which is consistent with the result in Fig. 8a.

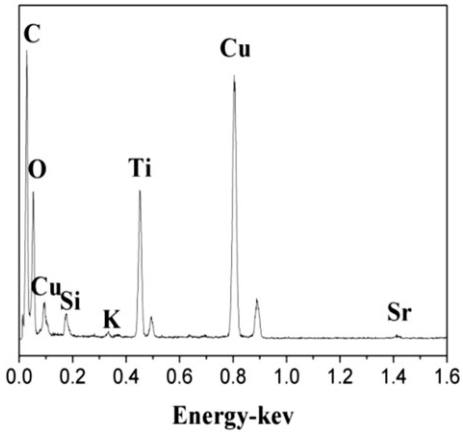

Fig. 5. EDX results of TiO_2–SrO core–shell films.

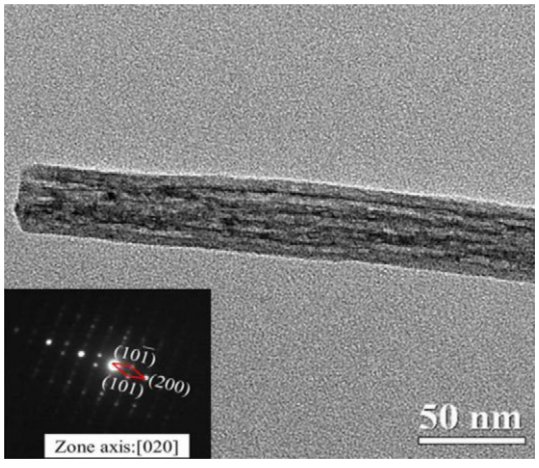

Fig. 4. TEM of TiO_2 NW prepared at 180 °C for 22 h in 8 M KOH. The inset shows the corresponding SAED patterns.

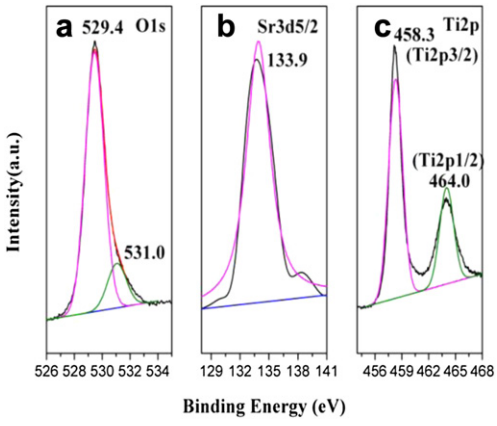

Fig. 6. XPS spectra of the as-prepared sample with an SrO shell, (a) O 1*s* spectrum; (b) Sr 3*d*5/2 spectra; (c) Ti 2*p* spectra.

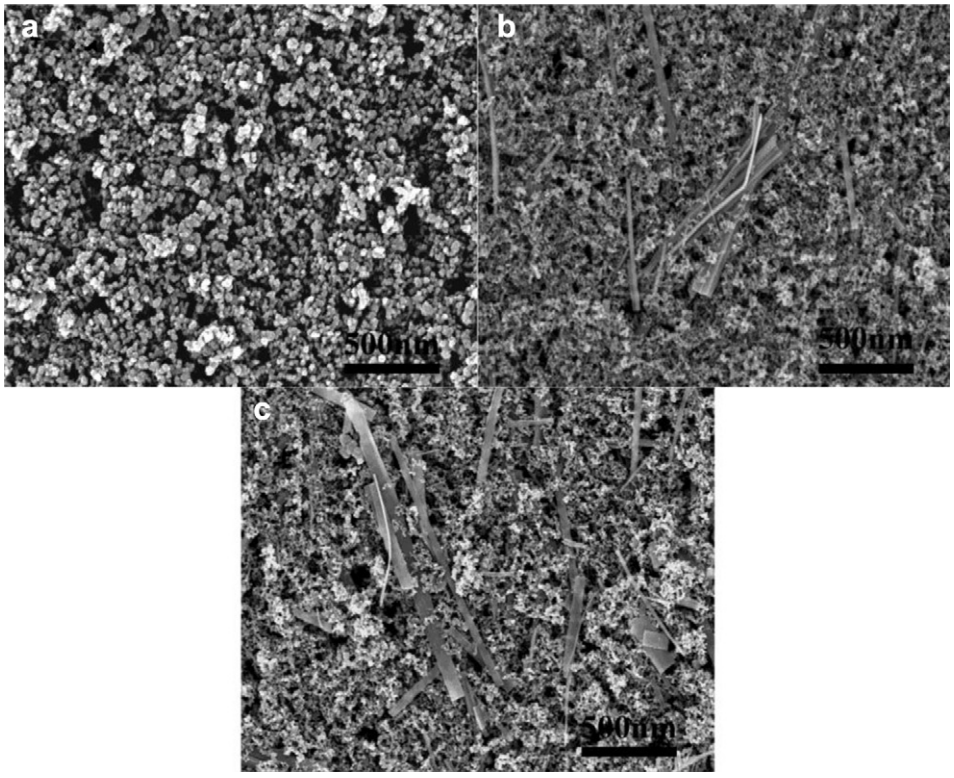

Fig. 7. SEM images of films with (a) PW0, (b) PW10, and (c) PW20.

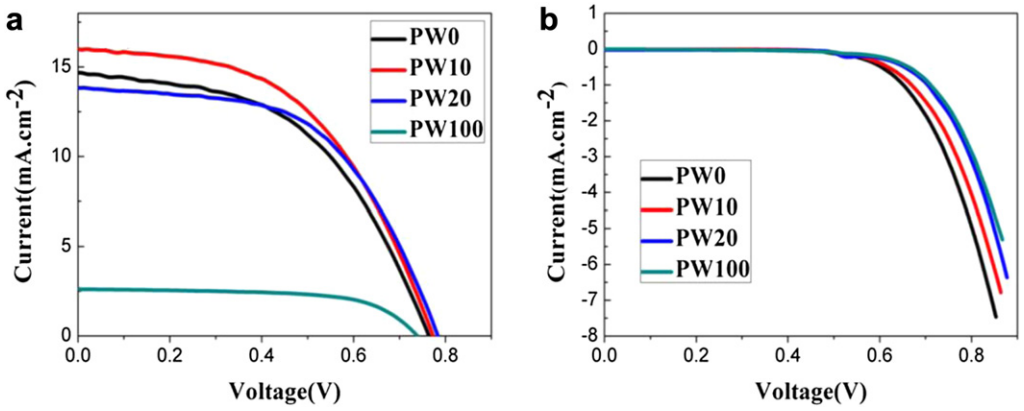

Fig. 8. *I–V* curves of DSSCs consisting of PW0, PW10, PW20, and PW100 photoanode under AM 1.5 (a) and under dark condition (b).

To explore the difference in the interfacial characteristics of the photoanodes, electrochemical impedance spectroscopy (EIS) of DSSCs was carried out under AM 1.5 at bias of V_{oc} and the frequency ranges from 0.1 Hz to 10^5 Hz with AC amplitude of 10 mV. Fig. 9 shows EIS of DSSCs consisting of PW0, PW10, PW20, and PW100. It can be found from Fig. 9a that three well-defined semicircles is shown in the high frequency region (>1 kHz), the middle region (1000–1 Hz) and the low region (1–0.1 Hz). The middle frequency in Nyquist is assigned to the charge transport resistance R_t and charge recombination resistance R_{ct}. However, under high illumination, such as AM 1.5, owing to high electron density in the conduction band of TiO_2, the charge transport R_t usually became negligible and the Nyquist curve in the middle frequency is reduced to a simple arc generated by the capacitance of TiO_2 paralleled with the charge recombination resistance R_{ct}. Therefore, the second semicircle in Nyquist plots only represents the charge recombination resistance [30]. And the larger charge recombination resistance implies the small recombination rate of electron with triioide, which is favorable to achieve higher cell performance [31–34]. The result shows that the cell with PW0 has the smallest semicircle in

Table 1
Performance parameters of DSSCs consisting of PW0, PW10, PW20, and PW100 photoanode.

Cell	V_{oc} (V)	J_{sc} (mA cm^{-2})	Fill factor (%)	Efficiency (%)
PW0	0.773	14.68	49.52	5.62
PW10	0.780	16.02	50.18	6.27
PW20	0.791	13.82	54.52	5.96
PW100	0.751	2.61	62.75	1.23

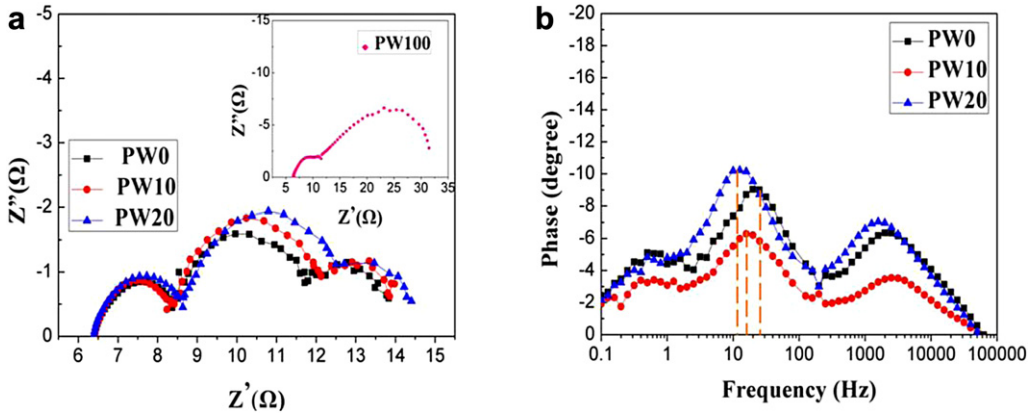

Fig. 9. EIS of DSSCs with different photoanodes: (a) Nyquist diagram, (b) Bode diagram. The inset shows the EIS spectra of PW100 electrodes.

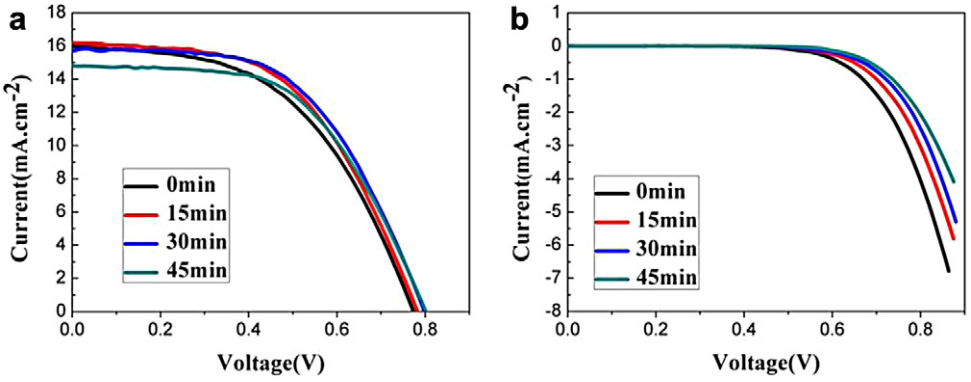

Fig. 10. *I–V* curves of DSSCs based on NWs/nanoparticles TiO_2 composite photoanodes with SrO shell under AM 1.5 (a) and under dark condition (b).

the middle frequency, while the semicircle of PW100 (inset) has the largest. The increase in the radius of the middle frequency semicircle in the Nyquist plot reveals the reduced electron recombination at the TiO_2/dye/electrolyte interface, which is crucial to achieve a higher overall cell performance. Fig. 9b shows the Bode phase plots of the EIS results. It is clear that the characteristic peak frequency of the PW0, PW10, and PW20 cell distribute from different values. The lifetime of photoelectrons (τ) can be calculated according to the following equation:

$$\tau_e = \frac{1}{2\pi f_{mid}} \quad (1)$$

here f_{mid} is the characteristic peak frequency at the medium frequency region. From the result we can learn that the value of f_{mid} decreases with the increase of NWs content indicating, the incorporation of nanowires into nanoparticles can prolong the electrons lifetime, which is in agreement with discussion above.

3.7.2. Cell with NWs/NPs and SrO shell

In order to investigate the role of SrO shell coating on the cell performance, PW10 photoanode is used for comparison. SrO shell coatings with different thickness are prepared by controlling the dipping time. *I–V* curves of DSSCs of PW10 with different SrO shell coatings are shown in Fig. 10. The corresponding cell performance parameters are also summarized in Table 2. The result shows that SrO shell coating on TiO_2 nano-composites can result in improvement in both V_{oc} and fill factor. With the increase of the shell thickness, V_{oc} increases from 0.780 V to 0.807 V, and the fill factor increases from 50.18% to 54.97%. The trend in J_{sc} is just a little complex. It first increases from 16.02 to16.20 mA cm^{-2} for dipping time of 15 min and then falls to 14.81 mA cm^{-2} with the increase of the dipping time up to 45 min. The explanation to this phenomenon is that electron injection is less efficient through the thick SrO shell coating compared with the uncoated sample, since the probability of electron tunneling decreases with the tunneling

Table 2
Performance parameters of DSSCs consisting of PW10 with different SrO shell coating.

Dipping time (min)	V_{oc} (V)	J_{sc} (mA cm^{-2})	Fill factor (%)	Efficiency (%)
0	0.780	16.02	50.18	6.27
15	0.789	16.20	52.65	6.73
30	0.803	15.71	54.78	6.91
45	0.807	14.81	54.97	6.57

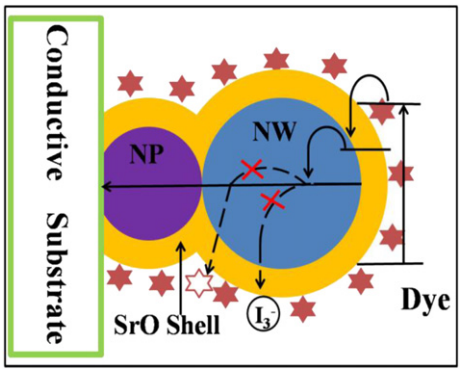

Fig. 11. Schematic view of an SrO–TiO_2 core–shell composites in cross section.

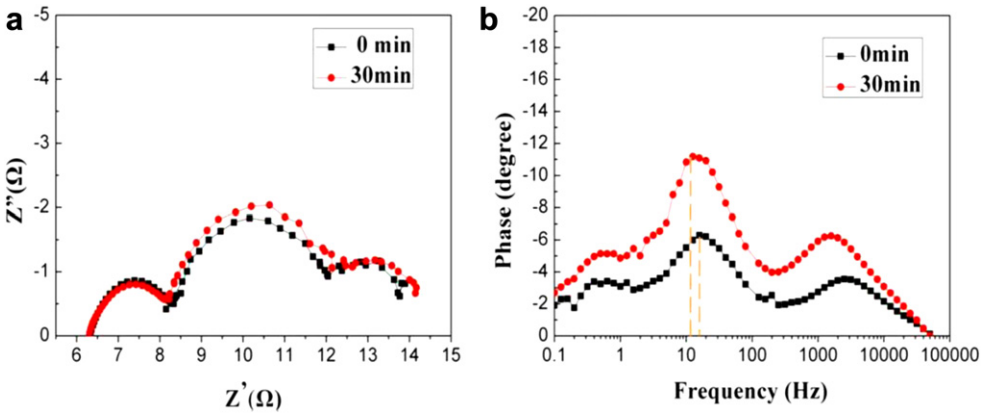

Fig. 12. EIS spectra of the DSSCs of cell PW10, PW10/SrO: (a) Nyquist diagram, (b) Bode diagram.

length exponentially [35,36]. However, the overall conversion efficiency increases from 6.27% to 6.91% (dipping 30 min). The cell performance confirms that suitable coating TiO_2 composite with SrO shell can suppress the charge recombination process effectively and improve the overall conversion efficiency. Fig. 10b shows that the dark current of the cells decrease with the increasing of the shell thickness, which suggests that the improvement in V_{oc} and fill factor result from a suppression of the charge recombination by SrO shell coating. The role and the mechanism of the wide-band semiconductor as shell coating on TiO_2 have been discussed in many researches [37–40]. The present study shows that the thin SrO shell coating can suppress the charge recombination, while thick SrO shell coating will reduce the cell's photocurrent by reducing the electron injection efficiency. As shown in Fig. 11, since SrO has a conduction band more negative than that of TiO_2, SrO shell coating on TiO_2 surface can form an energy barrier on the surface of photoanode, which can suppress the injected electrons from recombination with oxidized dye or I_3, thus reduces the charge recombination process and increases the conversion efficiency [39–43]. However, if the barrier layer is too thick, it will reduce the electron injection efficiency and then decrease the cell's photocurrent. Generally, it can be found that reasonable thickness of the shell layer is beneficial to suppress the recombination process and achieve relative high conversion efficiency.

Fig. 12 shows EIS of the cells of PW10 with and without SrO shell coating. The result also confirms that DSSC with SrO shell coating has less electron recombination at the TiO_2/dye/electrolyte interface and longer electron lifetime compared with the uncoated DSSC, as analysis in Fig. 11. Thus the application of SrO shell coating on NWs/NPs composite photoanode can promote the interfacial electron transfer and suppress the electron recombination effectively.

4. Conclusions

TiO_2 nanowires/nanoparticles composite photoanode with SrO shell coating is prepared for high performance DSSC. The reasonable ratio of nanowires and nanoparticles can promote the electron transfer and provide high surface area for dye adsorption. DSSC with 10 wt% nanowires (PW10) obtains a conversion efficiency of 6.27%. And SrO shell coating on the nano-composite photoanode can further improve the conversion efficiency to 6.91% because the shell coating can suppress the electron recombination effectively. The research finds that such a novel photoanode structure can suppress the electrons recombination process and increase the conversion efficiency effectively.

Acknowledgements

This research is financially supported by Natural Science Foundation of China (50902056). The authors would like to thank Materials Characterization Center of Huazhong University of Science and Technology for XRD, SEM, TEM, and XPS assistance.

References

[1] B.O. Regan, M. Grätzel, Nature 353 (1991) 737–740.
[2] M. Grätzel, Nature 414 (2001) 338–344.
[3] K. Park, Q.F. Zhang, B.B. Garcia, X.Y. Zhou, Y.H. Jeong, G.Z. Cao, Advanced Materials 22 (2010) 2329–2332.
[4] J.T. Jiu, S.J. Isoda, F.M. Wang, M. Adachi, Journal of Physical Chemistry B 110 (2006) 2087–2092.
[5] S. Ngamsinlapasathian, S. Sakulkhaemaruethai, S. Pavasupree, A. Kitiyanan, Journal of Photochemistry and Photobiology A 164 (2004) 145–151.
[6] Y. Sanehira, S. Uchida, Kagaku Kogyo 55 (2004) 796–800.
[7] J.B. Baxter, E.S. Aydil, Applied Physics Letters 86 (2005) 053114.
[8] M. Guo, P. Diao, S. Cai, Applied Surface Science 249 (2005) 71–75.
[9] J. Jiu, F. Wang, S. Isoda, M. Adachi, Chemistry Letters 34 (2005) 1506–1507.
[10] M. Law, L.E. Greene, J.C. Johnson, R. Saykally, Nature Materials 4 (2005) 455–459.
[11] T. Kurata, Y. Mori, S.J. Isoda, J.T. Jiu, K. Tsuchiya, F. Uchida, M. Adachi, Current Nanoscience 6 (2010) 269–276.
[12] B.V. Bergeron, A. Marton, G. Oskam, G.J. Meyer, Journal of Physical Chemistry B 109 (2005) 937–943.
[13] S. Chappel, S.G. Chen, A. Zaban, Langmuir 18 (2002) 3336–3342.
[14] S. Lee, J.Y. Kim, S.H. Youn, M. Park, K.S. Hong, H.S. Jung, J.-K. Lee, H. Shin, Langmuir 23 (2007) 11907–11910.
[15] S.J. Wu, H.W. Han, Q.D. Tai, J. Zhang, B.L. Chen, S. Xu, C.H. Zhou, Y. Yang, H. Hu, X.Z. Zhao, Applied Physics Letters 92 (2008) 122106–122108.
[16] I. Bedja, P.V. Kamat, Journal of Physical Chemistry 99 (1995) 9182–9188.
[17] K. Tennakone, G.R.R.A. Kumara, I.R.M. Kottegoda, V.P.S. Perera, Chemical Communications (1999) 15–16.
[18] H. Tada, A. Hattori, Y. Tokihisa, K. Imai, N. Tohge, S. Ito, Journal of Physical Chemistry B 104 (2000) 4585–4587.
[19] H.G. Yang, H.C. Zeng, Journal of American Chemical Society 127 (2005) 270–278.
[20] M. Gillet, R. Delamare, E. Gillet, Journal of Crystal Growth 279 (2005) 93–99.
[21] Y.J. Zhuo, C.C. Wu, S. Han, B. Chi, J. Pu, J. Tetsuro, J. Li, Journal of Nanoscience and Nanotechnology 11 (2011) 2298–2304.
[22] C.B. Azzoni, M.C. Mozzati, A. Paleari, V. Massarotti, D. Capsoni, M. Bini, Zeitschrift fuer Naturforschung, A: Physical Sciences 53 (1998) 693–698.
[23] X. Chen, L. Liu, P.Y. Yu, S.S. Mao, Science 331 (2011) 746–750.
[24] H. van Doveren, J.A. Verhoeven, The Journal of Electron Spectroscopy and Related Phenomena 21 (1980) 265–273.
[25] V. Young, T. Otagawa, Applied Surface Science 20 (1985) 228–248.
[26] J.C. Dupin, D. Gonbeau, P. Vinatier, A. Levasseur, Physical Chemistry Chemical Physics 2 (2000) 1319–1324.
[27] T. Lin, Z. Pi, M.C. Gong, J.B. Zhong, J.L. Wang, Y.Q. Chen, Chinese Chemical Letters 18 (2007) 241–243.
[28] M.S. Lazarus, T.K. Sham, Chemical Physics Letters 92 (1982) 670–674.
[29] B. Tan, Y.Y. Wu, Journal of Physical Chemistry B 110 (2006) 15932–15938.
[30] C.P. Hsu, K.M. Lee, J.T.W. Huang, C.Y. Lin, C.H. Lee, L.P. Wang, S.Y. Tsai, K.C. Ho, Electrochimica Acta 53 (2008) 7514–7522.
[31] S.J. Wu, H.W. Han, Q.D. Tai, J. Zhang, S. Xu, C.H. Zhou, Y. Yang, H. Hu, B.L. Chen, X.Z. Zhao, Journal of Power Sources 182 (2008) 119–123.

[32] J. Bisquert, Journal of Physical Chemistry B 106 (2002) 325–333.
[33] M. Adachi, M. Sakamoto, J. Jiu, Y. Ogata, S. Isoda, Journal of Physical Chemistry B 110 (2006) 13872–13880.
[34] Q. Zheng, H. Kang, J. Yun, J. Lee, J.H. Park, S. Baik, ACS Nano 5 (2011) 5088–5093.
[35] J. Frenkel, Physical Review 36 (1930) 1604–1618.
[36] G. Binning, H. Rohrer, C. Gerber, E. Weibel, Physical Review Letters 59 (1982) 57–61.
[37] Y. Diamant, S.G. Chen, O. Melamed, A. Zaban, Journal of Physical Chemistry B 107 (2003) 1977–1981.
[38] Matt Law, Lori E. Greene, Journal of Physical Chemistry B 110 (2006) 22652–22663.
[39] S.G. Chen, S. Chappel, Y. Diamant, A. Zaban, Chemistry of Materials 13 (2001) 4629–4634.
[40] J. Kruger, U. Bach, M. Grätzel, Advanced Materials 12 (2000) 447–451.
[41] S. Burnside, J.E. Moser, K. Brooks, M. Grätzel, D. Cahen, Journal of Physical Chemistry B 103 (1999) 9328–9332.
[42] F. Lenzmann, J. Krueger, S. Burnside, K. Brooks, M. Grätzel, D. Gal, S. Rühle, D. Cahen, Journal of Physical Chemistry B 105 (2001) 6347–6352.
[43] A. Vilan, A. Shanzer, D. Cahen, Nature 404 (2000) 166–168.